nanomaterials

MDPI

Article

Support Effects on the Activity of Ni Catalysts for the Propane Steam Reforming Reaction

Aliki Kokka [1], Athanasia Petala [2] and Paraskevi Panagiotopoulou [1,*]

[1] School of Chemical and Environmental Engineering, Technical University of Crete, 73100 Chania, Greece; akokka@isc.tuc.gr
[2] Department of Chemical Engineering, University of Patras, 26504 Patras, Greece; natpetala@chemeng.upatras.gr
* Correspondence: ppanagiotopoulou@isc.tuc.gr; Tel.: +30-28210-37770

Abstract: The catalytic performance of supported Ni catalysts for the propane steam reforming reaction was investigated with respect to the nature of the support. It was found that Ni is much more active when supported on ZrO_2 or YSZ compared to TiO_2, whereas Al_2O_3_ and CeO_2-supported catalysts exhibit intermediate performance. The turnover frequency (TOF) of C_3H_8 conversion increases by more than one order of magnitude in the order Ni/TiO_2 < Ni/CeO_2 < Ni/Al_2O_3 < Ni/YSZ < Ni/ZrO_2, accompanied by a parallel increase of the selectivity toward the intermediate methane produced. In situ FTIR experiments indicate that CH_x species produced via the dissociative adsorption of propane are the key reaction intermediates, with their hydrogenation to CH_4 and/or conversion to formates and, eventually, to CO, being favored over the most active Ni/ZrO_2 catalyst. Long term stability test showed that Ni/ZrO_2 exhibits excellent stability for more than 30 h on stream and thus, it can be considered as a suitable catalyst for the production of H_2 via propane steam reforming.

Keywords: propane steam reforming; H_2 production; Ni; TiO_2; CeO_2; YSZ; ZrO_2; Al_2O_3; drifts

check for updates

Citation: Kokka, A.; Petala, A.; Panagiotopoulou, P. Support Effects on the Activity of Ni Catalysts for the Propane Steam Reforming Reaction. *Nanomaterials* **2021**, *11*, 1948. https://doi.org/10.3390/nano11081948

Academic Editors: Nikolaos Dimitratos and Alberto Villa

Received: 30 June 2021
Accepted: 27 July 2021
Published: 28 July 2021

Publisher's Note: MDPI stays neutral with regard to jurisdictional claims in published maps and institutional affiliations.

Copyright: © 2021 by the authors. Licensee MDPI, Basel, Switzerland. This article is an open access article distributed under the terms and conditions of the Creative Commons Attribution (CC BY) license (https://creativecommons.org/licenses/by/4.0/).

1. Introduction

The high energy efficiency of fuel cells has drawn considerable attention toward the development of hydrogen production technologies. Hydrogen can be produced from fossil fuels either via hydrocarbon pyrolysis or hydrocarbon reforming processes including steam reforming, partial oxidation or autothermal reforming [1–5]. Biomass processes consisting of biological (bio-photolysis, dark fermentation, photo fermentation) and thermochemical (pyrolysis, gasification, combustion, liquefaction) methods as well as water splitting processes such as electrolysis, thermolysis or photolysis can be alternatively applied for the production of H_2 from renewable energy sources [2,6]. However, the latter approaches are facing some major obstacles mostly related to high cost and low H_2 yields. Currently, steam reforming of light hydrocarbons, including natural gas, ethane, propane, butane and liquified petroleum gas (LPG), are considered among the most promising and economical routes for hydrogen production [7]. Propane, which is the main component of LPG, has many advantages such as high energy density, compressibility to a transportable liquid at normal temperature and well-developed infrastructure which enable its use worldwide [8–10]. Moreover, propane can be stored and transferred as LPG through a wide distribution network or in high pressure cylinders in order to be supplied in remote places (e.g., agricultural, inaccessible or camping areas) or for domestic uses (e.g., households) [3,7].

Under propane steam reforming conditions, the water-gas shift reaction occurs simultaneously at low temperatures contributing to H_2 and CO_2 production, whereas CO/CO_2 methanation may also run in parallel yielding CH_4 and H_2O. Methane can be also formed via hydrogenation of CH_x species derived by the dissociative adsorption of propane on the catalyst surface or through propane decomposition accompanied by ethylene production. In certain cases, the C_2H_4, CH_4 and CO thus produced are further decomposed

leading to the formation of coke on the catalyst surface and consequently, to its progressive deactivation [11,12].

Supported noble metal (Rh, Ru, Pt, Pd) catalysts have been proposed to efficiently catalyze the production of H_2 via propane steam reforming exhibiting high resistance to coke formation [3,11,13,14]. However, the high cost and low availability of noble metals are major drawbacks restricting their use in practical applications [15–17]. Noble metals can be replaced by nickel, which is less expensive and able to convert propane with high H_2 yields. However, Ni is susceptible to coke formation and particles sintering considered to be responsible for catalyst deactivation [5,10,17]. The lifetime of Ni-based catalysts can be improved by optimization of the reaction conditions, catalyst promotion, improvement of the catalyst synthesis method as well as by the proper selection of the support [3,9,10,12,16,18,19].

Regarding the support material, it has been proposed that metal oxides characterized by high oxygen storage capacity, such as CeO_2, YSZ, TiO_2, ZrO_2 or CeO_2-ZrO_2, are able to suppress carbon deposition through the participation of their lattice oxygen in carbon removal [3,16]. Moreover, Ni catalysts supported on metal oxides or promoted metal oxides, which favor steam adsorption and mobility of surface hydroxyls, have been found to facilitate coke gasification [17,20].

Metal-support interactions have been also reported to impose a dramatic effect on both carbon deposition and metal particles sintering under conditions of hydrocarbons reforming [5,21,22]. It was demonstrated that stronger interactions between Ni and $MgAl_2O_4$ support resulted in high Ni dispersion and inhibition of the formation of large Ni clusters [22], whereas weak interactions between Ni and SiO_2 carrier were found to accelerate sintering and coke formation [21].

Therefore, the economic viability and practical applicability of H_2 production via propane steam reforming may be facilitated by the development of efficient Ni catalysts supported on suitable metal oxides, which will be able to possess both high activity and resistance against carbon deposition and particles sintering to realize economically viable reforming processes. In the present study the effect of the nature of the support (TiO_2, CeO_2, Al_2O_3, YSZ, ZrO_2) on the activity and selectivity of Ni-based catalysts for the propane steam reforming reaction was investigated. Mechanistic aspects related to the support influence on the reaction pathway were also studied and are discussed.

2. Materials and Methods

2.1. Catalyst Preparation and Characterization

The wet impregnation method was applied to prepare Ni (5 wt.%) catalysts supported on commercial metal oxide powders by using an aqueous solution of Ni ($Ni(NO_3)_2 \cdot 6H_2O$) as the metal precursor salt. The commercial metal oxide carriers were used as received and were (a) activated aluminum oxide (Al_2O_3), catalyst support, 99% (metals basis) (Alfa Aesar, Kandel, Germany), (b) AEROXIDE® TiO_2 P25 (TiO_2) (Evonik Industries AG, Essen, Germany), (c) cerium (IV) oxide (CeO_2), nanopowder, 99.5% min (Alfa Aesar, Kandel, Germany), (d) yttria-stabilized zirconia (YSZ) (8Y-SZ, Tosoh, Amsterdam, The Netherlands) and (e) zirconium (IV) oxide (ZrO_2) 99% (metal basis) (Alfa Aesar, Kandel, Germany). The resulting materials were dried at 110 °C for 24 h followed by reduction at 400 °C under H_2 flow for 2 h. The selection of reducing Ni catalysts at 400 °C for 2 h was based on previous studies which indicated that under these reducing conditions nickel oxide species are able to be completely converted to metallic nickel [23–25].

The X-ray diffraction patterns of the catalysts were recorded using an X-ray powder diffractometer (A Brucker D8 Advance instrument, Bruker, Karlsruhe, Germany) using Cu K_a radiation (λ = 0.15406 nm, 40 kV, 40 mA) and a scan rate of 0.025°/s over a range of 2θ between 20 and 80°. The diffraction pattern was identified by comparison with those

supplied from the JCPDS data base, whereas the primary crystallite size of M_xO_y (d_{MxOy}) was estimated according to Scherrer's equation:

$$d_{M_xO_y} = \frac{0.9 \cdot \lambda}{B \cdot \cos\theta} \quad (1)$$

where θ is the angle of diffraction corresponding to the peak broadening, B is the full-width at half maximum intensity (in radians) and λ = 0.15406 nm is the X-ray wavelength corresponding to CuK_a radiation.

The specific surface area (SSA) of the supported Ni catalysts were measured by N_2 adsorption at 77 K (B.E.T. technique) using a Gemini III 2375 instrument (Micromeritics, Norcross, GA, USA). Carbon monoxide chemisorption measurements at 25 °C were applied for the determination of Ni dispersion and mean particle size using a modified Sorptomatic 1900 apparatus (Fisons Instruments, Glaskow, UK) and assuming a CO:Me stoichiometry of 1:1, an atomic surface area of 6.5 $Å^2$ and spherical particles. CO chemisorption measurements were used instead of H_2 chemisorption in order to avoid overestimation of Ni dispersion due to hydrogen spillover effects, which have been previously found to occur over supported Ni catalysts [26,27]. Nickel particle size was calculated according to the following equation:

$$d_{Ni} = \frac{60000}{\rho_{Ni} \cdot S_{Ni}} \text{ [Å]} \quad (2)$$

where d_{Ni} is the mean crystallite diameter, ρ_{Ni} (= 8.9 g·cm^{-3}) is the density of Ni and S_{Ni} [m^2/g_{Ni}] is the surface area per gram of Ni.

Transmission electron microscopy (TEM) images were obtained with a JEM-2100 system (JEOL, Akishima, Tokyo, Japan) operated at 200 kV (point resolution 0.23 nm) using an Erlangshen CCD Camera (Model 782 ES500W, Gatan Inc., Pleasanton, CA, USA). Samples were dispersed in water and spread onto a carbon-coated copper grid (200 mesh). Details related to the equipment and procedures used for catalyst characterization have been described in detail elsewhere [28].

2.2. Catalytic Performance Tests and Kinetic Measurements

The catalytic performance of the synthesized materials was studied in a tubular fixed-bed quartz reactor under atmospheric pressure using an apparatus which has been described in detail elsewhere [11]. The reaction conditions were as follows: temperature range 400–750 °C, H_2O/C = 3.25, and gas hourly space velocity (GHSV) = 55,900 h^{-1}. The reactor was loaded with 150 mg of catalyst (particle diameter: 0.15 < d_p < 0.25 mm) and placed in an electric furnace, where it was reduced in situ at 300 °C for 1 h under 50%H_2/He flow (60 cm^3 min^{-1}) to ensure that the Ni exists in its metallic phase prior to catalytic performance tests. Catalyst reduction was followed by heating at 750 °C under He and subsequent switch of the flow to the feed stream consisted of 4.5%C_3H_8 + 0.15%Ar + 44%H_2O (He balance). Argon was used as internal standard in order to account for the volume change. Water was fed through an HPLC pump (LD Class Pump, TELEDYNE SSI, PA, USA) into a vaporizer maintained at 180 °C and mixed with the gas stream coming from mass-flow controllers. A condenser immersed in an ice bath was placed at the exit of the reactor to condensate water prior to introduction of the gas stream to the analysis system. Reaction gases (He, 30%C_3H_8−1%Ar/He, H_2) are supplied from high-pressure gas cylinders (Buse Gas, Bad Hönningen, Germany) and are of ultrahigh purity. Measurements of reactants' and products' concentrations were obtained by stepwise decreasing temperature up to 400 °C. The effluent from the reactor was analyzed using two gas chromatographs (Shimadzu, Kyoto, Japan) which were connected in parallel. The procedure used for gas phase analysis was described in our previous study [11]. The conversion of propane ($X_{C_3H_8}$) was calculated using the following expression:

$$X_{C_3H_8} = \frac{[\text{Carbon}]_{\text{total,out}}}{[\text{Carbon}]_{\text{total,out}} + [C_3H_8]_{\text{out}}} \times 100 \quad (3)$$

where $[\text{Carbon}]_{\text{total,out}}$ is the sum of the concentrations of all carbon containing products:

$$[\text{Carbon}]_{\text{total,out}} = \frac{[\text{CO}] + [\text{CO}_2] + [\text{CH}_4]}{3} + 2 \times \frac{[\text{C}_2\text{H}_4] + [\text{C}_2\text{H}_6]}{3} \quad (4)$$

Selectivity toward reaction products containing carbon was defined using Equation (5). The factor *n* corresponds to the number of carbon atoms in the corresponding molecule (e.g., for CO is 1, for C_2H_4 is 2 etc.):

$$S_{\text{Cn}} = \frac{[\text{C}_\text{n}] \times \text{n}}{3 \times [\text{Carbon}]_{\text{total,out}}} \times 100 \quad (5)$$

Selectivity toward hydrogen production was defined as the concentration of hydrogen produced divided with the concentration of all products containing hydrogen according to Equation (6). The factor m represents the number of hydrogen atoms in the corresponding molecule (e.g., for CH_4 and C_2H_4 is 4).

$$S_{\text{H}_2}(\%) = \frac{[\text{H}_2]}{[\text{H}_2] + \text{m}/2 \times [\text{C}_\text{n}\text{H}_\text{m}]} \times 100 \quad (6)$$

The intrinsic reaction rates for propane steam reforming reaction were measured for low propane conversions ($X_{C_3H_8}$< 10%) by varying W/F using the following expression:

$$R_{\text{C}_3\text{H}_8} = \frac{[\text{C}_3\text{H}_8]_{\text{in}} \cdot \text{F}_{\text{in}} - [\text{C}_3\text{H}_8]_{\text{out}} \cdot \text{F}_{\text{out}}}{\text{W}} \times 100 \quad (7)$$

where R_{C3H8} is the molar rate of C_3H_8 consumption (mol s^{-1} $g_{cat}{}^{-1}$), $[C_3H_8]_{in}$, $[C_3H_8]_{out}$, are the inlet and outlet concentrations (*v*/*v*) of C_3H_8, respectively, F_{in} and F_{out} are the total flow rates in the inlet and outlet of the reactor ($mols^{-1}$), respectively, and W is the mass of catalyst (g_{cat}).

Turnover frequencies (TOFs) of propane conversion were estimated following Equation (8) taking into account the measurements of both the reaction rates and nickel dispersions:

$$\text{TOF} = \frac{R_{\text{C}_8\text{H}_8} \cdot \text{AW}_{\text{Ni}}}{\text{D}_{\text{Ni}} \cdot \text{X}_{\text{Ni}}} \quad (8)$$

where AW_{Ni} is the atomic weight of nickel (g_{Ni}/mol_{Ni}), X_{Ni} is the nickel loading (g_{Ni}/g_{cat}) and D_{Ni} is the dispersion of nickel.

2.3. In Situ FTIR Spectroscopy

In situ Fourier transform infrared (FTIR) experiments were carried out using an iS20 FTIR spectrometer (Nicolet, Thermo Fischer Scientific, Waltham, MA, USA) equipped with an MCT detector, a KBr beam splitter and a diffuse reflectance (DRIFT) sampling system (Specac, Orpington, UK) accompanied by an environmental chamber suitable for the study of diffusely reflecting solid samples in a controlled atmosphere. A flow system equipped with mass flow controllers, a steam saturator and a set of valves used for controlling the gas stream interacted with the catalyst surface, was directly connected to the gas inlet of the environmental chamber.

In a typical experiment, the catalyst powder was placed in the sampling system and heated at 500 °C in flowing helium for 10 min and then reduced under hydrogen flow at 300 °C for 30 min. The flow was then switched to He and the temperature was increased at 500 °C. After remaining 10 min at this temperature the sample was cooled at 100 °C. While cooling, the background spectra were recorded at the desired temperatures. Finally, the flow was switched to the reaction mixture, which consisted of 0.5%C_3H_8 +5%H_2O (in He). Steam was introduced to the system via an independent He line passing through a saturator containing water maintained at 60 °C. The resulting gas mixture was fed to the DRIFT cell through stainless steel tubing maintained at 60 °C by means of heating tapes. A

spectrum was collected at 100 °C after 15 min-on-stream followed by a stepwise increase of temperature up to 500 °C. During heating, spectra were recorded at selected temperatures after an equilibration for 15 min. In all experiments, the total flow through the DRIFT cell was 30 cm^3 min^{-1}. Reaction gases (He, 2%C_3H_8/He, H_2) are supplied from high-pressure gas cylinders (Buse Gas, Bad Hönningen, Germany) and are of ultrahigh purity.

3. Results

3.1. Catalyst Characterization

The XRD patterns of Ni/M_xO_y catalysts are shown in Figure 1. The characteristic peaks located at the diffraction angles of 32.7°, 37.7°, 39.9°, 45.8° and 67.5° were appeared for Ni/Al_2O_3 which are attributed to (220), (311), (222), (400) and (440) facets of cubic Al_2O_3 (JCPDS Card No. 10-425), respectively. The XRD spectra recorded for Ni/CeO_2 catalyst consisted of peaks located at 2θ = 28.79°, 33.26°, 47.62°, 56.34°, 59.1°, 69.42°, 76.66°, 79.11° attributed to (111), (200), (220), (311), (222), (400), (331) and (420) planes of the cubic CeO_2 (JCPDS Card No. 2-1306), whereas in the case of Ni/ZrO_2 catalyst numerous peaks were detected on the XRD pattern. In particular, the peaks detected at 24.2°, 24.5°, 28.5°, 31.7°, 34.5°, 35.5°, 38.9°, 41.0°, 41.5°, 45.1°, 45.8°, 49.5°, 50.5°, 54.4°, 55.7°, 57.5°, 60.2°, 62.1°, 63.2°, 66.0°, 71.6°, 75.3° correspond to (011), (−110), (−111), (111), (002), (200), (021), (−211), (−121), (112), (211), (022), (−221), (202), (013), (212), (−302), (113), (311), (−321), (−104), (−140) planes of monoclinic ZrO_2 (JCPDS Card No. 13-307). When Ni was supported on YSZ, the XRD pattern was characterized by reflections at 30.4°, 35.1°, 50.4°, 59.9°, 62.9° and 74.0° attributed to (111), (200), (220), (311), (222) and (400) planes of YSZ (JCPDS Card No. 82-1246), respectively.

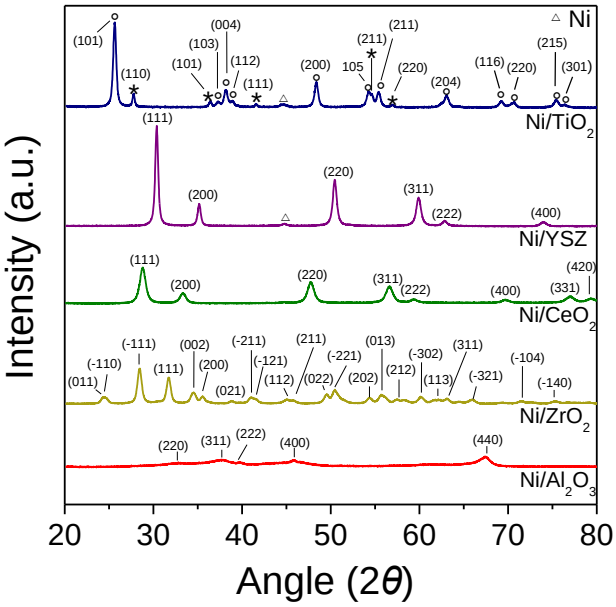

Figure 1. XRD patterns obtained from 5 wt.% Ni catalysts supported on the indicated commercial metal oxide carriers. The reflection planes of anatase (°) and rutile (*) TiO_2 phases are indicated in the diffractogram of Ni/TiO_2 catalyst.

Results obtained from Ni/TiO_2 catalyst showed that the sample consisted of TiO_2 in both its anatase and rutile form exhibiting peaks at 2θ = 25.6° (101), 37.2° (103), 38.2° (004), 38.9° (112), 48.4° (200), 54.3° (105), 55.4° (211), 63.1° (204), 69.3° (116), 70.7° (220), 75.4° (215) and 76.4° (301) for anatase (JCPDS Card No. 21-1272), and at 2θ = 27.6° (110), 36.3° (101), 41.6° (111), 44.3° (210), 54.6° (211), 56.9° (220) and 64.3° (310) for rutile (JCPDS Card No. 21-1276).

In the case of Ni/TiO_2 and Ni/YSZ catalysts an additional weak peak located 44.5° was appeared corresponding to Ni (111) plane (JCPDS Card No. 04-0850). The absence of

peaks corresponding to metallic Ni for the rest catalysts investigated is due to the low Ni loading and/or particle size. The primary crystallite size of the supports was estimated according to Scherrer's formula at the diffraction angles corresponding to (440) plane for Al_2O_3, (−111) plane for ZrO_2, (111) plane for CeO_2, (111) plane for YSZ and (101) plane for TiO_2, and it was found to be 6.0 nm for Ni/Al_2O_3, 10.5 nm for Ni/CeO_2, 15.0 nm for Ni/ZrO_2, 20.9 nm for Ni/YSZ and 21.8 nm for Ni/TiO_2 (Table 1).

The SSAs of Ni catalysts supported on metal oxide (M_xO_y) carriers were estimated equal to 39 m^2/g for Ni/ZrO_2, 11 m^2/g for Ni/YSZ, 66 m^2/g for Ni/Al_2O_3, 39 m^2/g for Ni/CeO_2 and 41 m^2/g for Ni/TiO_2 (Table 1).

Table 1. Physicochemical properties of supported Ni (5 wt.%) catalysts and their apparent activation energies for propane steam reforming reaction.

Catalyst	SSA [(a)] (m^2/g)	d_{MxOy} [(b)] (nm)	D_{Ni} [(c)] (%)	d_{Ni} [(c)] (nm)	Activation Energy (kJ/mol)
5%Ni/ZrO_2	39	15.0	5.7	17.8	154
5%Ni/YSZ	11	20.9	4.7	21.4	140
5%Ni/Al_2O_3	66	6.0	4.0	25.5	121
5%Ni/CeO_2	39	10.5	11.9	8.5	102
5%Ni/TiO_2	41	21.8	2.8	36.1	127

[(a)] Specific surface area, estimated with the BET method. [(b)] Primary crystallite size of M_xO_y, estimated from XRD line broadening. [(c)] Dispersion and mean particle size of Ni, estimated from selective chemisorption measurements.

Results of Ni dispersion (D_{Ni}) and mean particle size (d_{Ni}) estimated from CO chemisorption meaurements are summarized in Table 1. Generally, low Ni dispersions were estimated for all the investigated catalysts, most possibly due to the high Ni content (5 wt.%) in agreement with previous studies [4,6]. Higher Ni dispersion of 11.9% and smaller particle size of 8.5 nm was found for Ni/CeO_2 catalyst, whereas Ni/TiO_2 exhibited the lowest value of Ni dispersion of 2.8% and the largest particle size of 36.1 nm.

Figure 2 shows representative TEM images and selected area electron diffraction (SAED) patterns obtained from Ni/YSZ, Ni/CeO_2 and Ni/TiO_2 catalysts. In all cases Ni particles appear as fairly homogeneously distributed spherical particles with average sizes of 20 nm for Ni/YSZ, 10 nm for Ni/CeO_2 and 30 nm for Ni/TiO_2, in agreement with those estimated according to CO chemisorption measurements (Table 1).

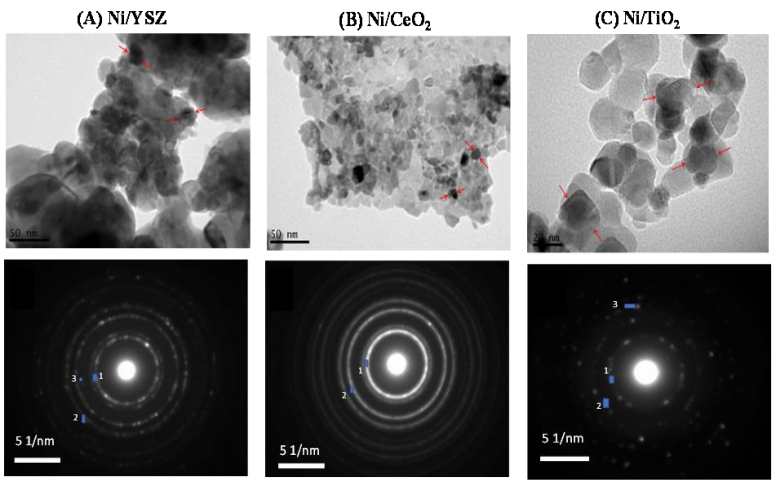

Figure 2. TEM images and Selected Area Electron Diffraction (SAED) patterns obtained for (**A**) 5%Ni/YSZ, (**B**) 5%Ni/CeO_2 and (**C**) 5%Ni/TiO_2 catalysts. Ni particles are indicated with red arrows.

It should be noted that, based on the results of Table 1, the mean particle size of Ni is similar to the average size of the corresponding metal oxide used as support for all the investigated catalysts. This may hinder distinguishing between Ni particles and the M_xO_y carrier in TEM images. Thus, SAED analysis was performed to calculate the d-spacing in an attempt to further discerned Ni particles from those of metal oxide support (Figure 2, Table 2). Results indicated that, in all cases, Ni particles are present in TEM images as evidenced by the appearance of the (111) plane of Ni ($d_{spacing}$ = 0.21 nm, JCPDS No 1-1258). The appearance of the (101) ($d_{spacing}$ = 0.35 nm, JCPDS No 1-562) and (103) ($d_{spacing}$ = 0.24 nm, JCPDS No 1-562) planes of TiO_2, the (111) ($d_{spacing}$ = 0.30 nm, JCPDS No 30-1468) and (200) ($d_{spacing}$ = 0.26 nm, JCPDS No 30-1468) planes of YSZ, as well as the (111) ($d_{spacing}$ = 0.31 nm, JCPDS No 1-800) and (200) ($d_{spacing}$ = 0.27 nm, JCPDS No 1-800) planes of CeO_2 also confirmed the presence of the metal oxides.

Table 2. Selected area electron diffraction (SAED) analysis of TEM images obtained for 5%Ni/YSZ, 5%Ni/CeO_2 and 5%Ni/TiO_2 catalysts.

Catalyst	Spot	d-Spacing (Å)	Formula	Crystallographic Plane (h k l)	JCPDS No
5%Ni/YSZ	1	3.0	$Y_{0.15}Zr_{0.85}O_{1.93}$	(111)	30-1468
	2	2.6	$Y_{0.15}Zr_{0.85}O_{1.93}$	(200)	30-1468
	3	2.1	Ni	(111)	1-1258
5%Ni/CeO_2	1	3.1	CeO_2	(111)	1-800
	2	2.7	CeO_2	(200)	1-800
	3	2.1	Ni	(111)	1-1258
5%Ni/TiO_2	1	3.5	TiO_2	(101)	1-562
	2	2.4	TiO_2	(103)	1-562
	3	2.1	Ni	(111)	1-1258

3.2. Influence of the Nature of the Support on Catalytic Activity

The influence of the nature of the support on catalytic performance for the propane steam reforming reaction has been investigated using Ni catalysts (5 wt.%) supported on five different commercial metal oxide powders (ZrO_2, YSZ, TiO_2, Al_2O_3, CeO_2). The results obtained are shown in Figure 3A, where propane conversion is plotted as a function of reaction temperature. It is observed that, among the investigated catalysts, Ni/ZrO_2 is the most active one, exhibiting measurable C_3H_8 conversions at temperatures higher than 400 °C and achieving complete conversion at 750 °C. Although Ni/YSZ is activated at similar temperatures as Ni/ZrO_2, the conversion curve of propane is shifted toward higher temperatures. This is also the case for Ni/Al_2O_3 and Ni/CeO_2 catalysts, which present similar performance. The latter catalysts are less active than Ni/YSZ below 550 °C, but are able to reach higher X_{C3H8} at higher temperatures. The titania-supported catalyst becomes active above 500 °C, with the propane conversion curve being shifted at remarkably higher temperatures. In all examined cases, the carbon balance was satisfactory, with a deviation of <1%.

Results of specific reaction rate measurements are presented in the Arrhenius diagram of Figure 3B, where it is observed that the TOF of propane conversion increases in the order Ni/TiO_2 < Ni/CeO_2 < Ni/Al_2O_3 < Ni/YSZ < Ni/ZrO_2, with its value at 450 °C being more than one order of magnitude higher when Ni is dispersed on ZrO_2 compared to TiO_2, and approximately 2.5 times higher than that of Ni/Al_2O_3. It should be mentioned that, as discussed above, the mean particle size of Ni varies significantly for the investigated catalysts from 8.5 nm for Ni/CeO_2 to 36.1 nm for Ni/TiO_2. If the Ni particle size were similar for this set of catalysts then the order of catalytic activity could be somewhat different. Interestingly, no trend was observed between the specific reaction rate and Ni particle size or M_xO_y crystallite size or M_xO_y surface area. This indicates that either

these parameters do not affect catalytic activity or most possibly each of them contributes in a different manner to the reaction rate, resulting in the observed catalyst ranking. It should be noted that all catalysts have been reduced at 400 °C prior to physicochemical characterization measurements. Although the values of SSA or d_{MxOy} or d_{Ni} may were different if catalyst pre-reduction was carried out at 750 °C, which is the onset reaction temperature for catalytic performance experiments, the trend of catalytic properties with respect to the nature of the support is not expected to vary due to the catalyst pretreatment at different temperatures, at least to such an extent that would affect the catalyst ranking for the propane steam reforming reaction.

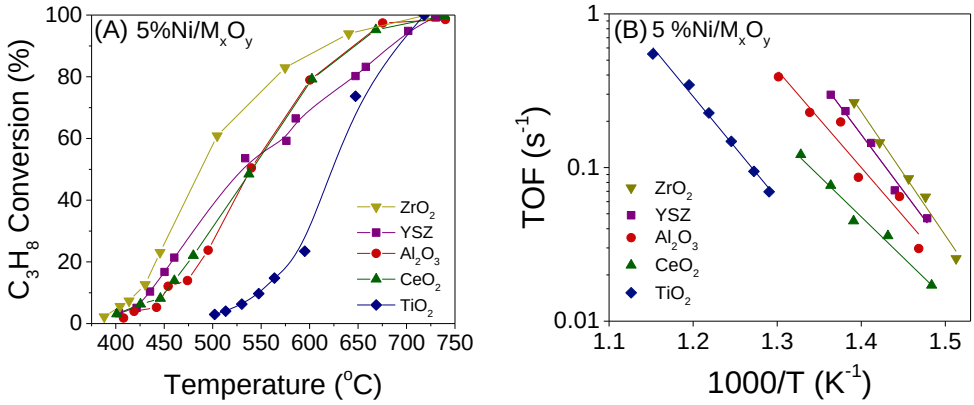

Figure 3. (**A**) Conversions of C_3H_8 as a function of reaction temperature and (**B**) Arrhenius plots of turnover frequencies of C_3H_8 conversion obtained over Ni catalysts (5.0 wt.%) supported on the indicated commercial oxide carriers. Experimental conditions: Mass of catalyst: 150 mg; particle diameter: $0.15 < d_p < 0.25$ mm; Feed composition: 4.5% C_3H_8, 0.15% Ar, 44% H_2O (balance He); Total flow rate: 250 cm^3 min^{-1}.

The apparent activation energies (E_a) of the propane steam reforming reaction were calculated from the slopes of the fitted lines of Figure 3B. The results showed that the nature of the metal oxide carrier significantly affects E_a, which takes values between 102 kJ/mol for Ni/CeO_2 and 154 kJ/mol for Ni/ZrO_2 without presenting any trend with respect to catalytic activity (Table 1). This can be explained taking into account that, as it will be discussed below, several reactions run in parallel under the present experimental conditions each one of which is influenced by the nature of the support in a different manner resulting in the observed random variation of E_a with catalytic activity. The results are in agreement with our previous study where it was found that the apparent activation energy for the reaction of steam reforming of propane over Rh catalysts supported on a variety of metal oxides does not present any trend with the activity order [11].

Figure 4 shows the selectivities toward reaction products as a function of temperature over the supported Ni catalysts investigated. In all cases the main products detected were H_2, CO_2, CO and CH_4 with their selectivities being significantly varied with temperature. In particular, for Ni/ZrO_2 catalyst (Figure 4A), both hydrogen (S_{H2}) and CO_2 (S_{CO2}) selectivities decrease from 99 to 78% and from 98 to 58%, respectively, with increasing temperature in the range of 390–505 °C followed by an increase of methane selectivity (S_{CH4}) up to 32.5%, indicating the occurrence of CO_2 methanation reactions. Carbon dioxide consumption continues with further increase of temperature above 505 °C contrary to S_{H2} which progressively increases reaching 99% at 720 °C. Consumption of CO_2 is followed by production of CO providing evidence that the reverse WGS (RWGS) reaction is enhanced at high temperatures. Moreover, S_{CH4} decreases above 505 °C and becomes practically zero at 720 °C, implying that the reaction of methane steam reforming occurs contributing to the observed increase of both S_{H2} and S_{CO}. It should be noted that selectivity toward reaction products containing carbon was defined as the concentration of each product containing carbon at reactor effluent over the concentration of all products containing

carbon (5), whereas S_{H2} was defined as the concentration of hydrogen produced divided by the concentration of all products containing hydrogen (6). Therefore, the values of Sc_n and S_{H2} cannot be correlated based on the stoichiometry of the reactions taking place under propane steam reforming conditions.

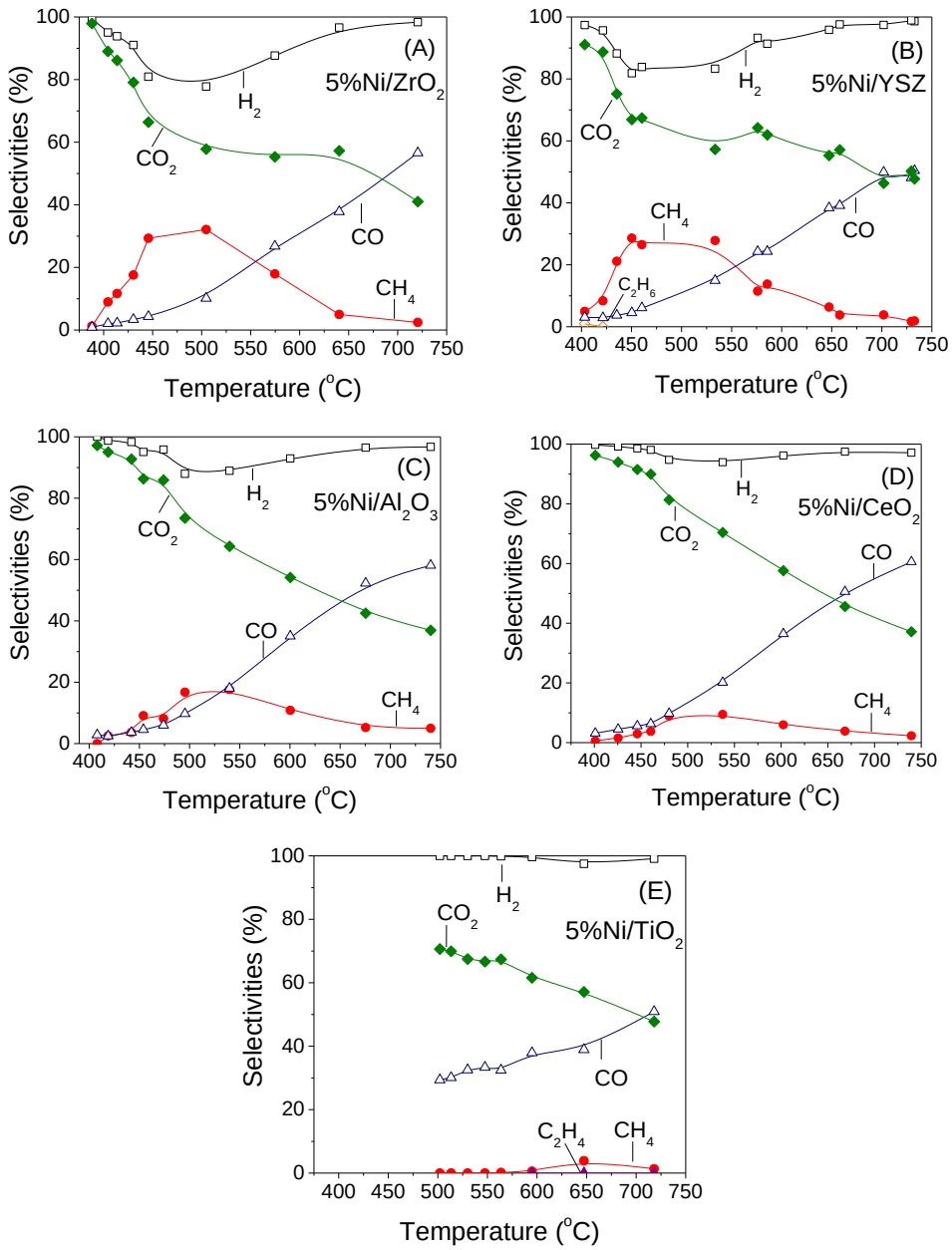

Figure 4. Selectivities toward reaction products as a function of reaction temperature obtained over Ni catalysts (5.0 wt.%) supported on (**A**) ZrO_2, (**B**) YSZ, (**C**) Al_2O_3, (**D**) CeO_2 and (**E**) TiO_2. Experimental conditions: same as in Figure 3.

Qualitatively similar results were obtained for the rest of the investigated Ni catalysts, with the main differences being related to the values of the selectivities toward the reaction products, which reflect the extent of each reaction taking place with respect to the nature of the support. In particular, the observed decrease of S_{H2} and S_{CO2} at low temperatures and the simultaneous increase of S_{CH4} are higher for the most active Ni/ZrO_2 (Figure 4A) and Ni/YSZ (Figure 4B) catalysts, followed by Ni/Al_2O_3 (Figure 4C) and Ni/CeO_2 (Figure 4D), whereas it is eliminated for Ni/TiO_2 (Figure 4E). As a result methane production increases in the order of $Ni/TiO_2 < Ni/CeO_2 < Ni/Al_2O_3 < Ni/YSZ < Ni/ZrO_2$ which is consistent

with the order of catalytic activity. This can be clearly seen in Figure 5 where the TOF at 450 °C is plotted as a function of methane selectivity obtained at the same temperature for all the investigated catalysts. It is observed that the specific reaction rate increases from 0.018 s^{-1} to 0.33 s^{-1} following the above catalyst ranking and accompanied by a parallel increase of S_{CH4} from 0 to 29%. The results indicate that there is a clear relationship between catalytic activity and methane production.

It should be noted that besides CO_2 hydrogenation, CH_4 can be also produced via CO hydrogenation. However, the contribution of the latter reaction does not seem to be significant for the results of the present study taking into account the low S_{CO} below 500 °C and its progressive increase with temperature. Moreover, methane formation may also take place via hydrogenation of CH_x species formed following the dissociative adsorption of propane on Ni surface and the subsequent hydrogenation of the so-formed C_3H_x species [29,30]. As it will be discussed below, the formation of CH_x species intermediates may be the key reaction since it has been proposed that they interact with the hydroxyl groups or lattice oxygen of the support producing CO or CO_2 and H_2 [3,29,30].

The mass of H_2 produced per propane mass unit contained in the feed was calculated at 550 °C and it was found to be higher for Ni/ZrO_2 (23.2 wt.%) followed by Ni/CeO_2 (21.2 wt.%), Ni/Al_2O_3 (20.6 wt.%) and Ni/YSZ (19.7 wt.%), whereas Ni/TiO_2 exhibits the lowest H_2 production (5.2 wt.%).

The influence of the nature of the support on the activity of Ni catalysts for propane steam reforming reaction was also investigated by Harshini et al. [16], who found that $Ni/LaAlO_3$ was more active than Ni/Al_2O_3, while Ni/CeO_2 exhibited intermediate performance. The optimum activity of the former catalyst was attributed to the small Ni nanoparticles dispersed on $LaAlO_3$ surface. Although the effect of the support nature on propane steam reforming activity has not been widely studied over Ni catalysts, certain properties of metal oxide carriers may help explain the results of Figure 3. For example, the use of YSZ as support, which exhibited high activity in the results of the present study, has been found to suppress carbon deposition over Rh-Ni catalysts by providing lattice oxygen, which facilitates carbon removal and enhances the dissociation of C-C bond under reaction conditions [3]. The prevention of coke formation, occurring either via hydrocarbons decomposition or CO dissociation, by the lattice oxygen of the support has been also demonstrated over Ni/CeO_2-Al_2O_3 [19]. Moreover, the addition of manganese oxide on Ni/Al_2O_3 was found to act as an oxygen donor that is transferred to Ni particles leading to rapid decomposition and oxidation of C_3H_8 and CH_4 or C_2H_4 that may be produced under reaction conditions, resulting in further H_2 production and improvement of the catalyst lifetime [9]. It has been also found that activation of steam followed by H_2 formation may be favored over metal catalysts supported on "reducible" metal oxides through generation of oxygen defects, resulting in improved propane steam reforming activity and resistance to coke formation [3,13,31]. Based on previous studies, the reducibility of the supports used in the present study is expected to vary significantly. It is well known that Al_2O_3 is a hardly reducible metal oxide characterized by low oxygen storage capacity contrary to TiO_2 and CeO_2, which are strongly reducible metal oxides, or ZrO_2 and YSZ, which are characterized by intermediate oxygen mobility [32]. Based on the above, Ni/TiO_2 should be also active for the title reaction, taking into account that titania support is characterized by high oxygen storage capacity [32,33]. However, the results of Figure 3 clearly show that: (a) this catalyst was the least active one and (b) the catalytic activity is increased in the order $Ni/TiO_2 < Ni/CeO_2 < Ni/Al_2O_3 < Ni/YSZ < Ni/ZrO_2$, which cannot be correlated with the reducibility of the support. Therefore, it is evident that support reducibility is not among the key parameters affecting the catalytic activity of Ni according to the results of the present study. The low activity of Ni/TiO_2 catalyst may be related to the fact that Ni/TiO_2 has lower Ni dispersion and larger Ni particles, which was previously suggested to suppress both propane steam reforming [15,16], and the intermediate (CO_2 or CH_x) hydrogenation reactions, in excellent agreement with the results of our previous study [28]. However, large Ni particles may not be solely responsible for the low activity of Ni/TiO_2

taking into account that no trend was observed between TOF and Ni particle size for the investigated catalysts.

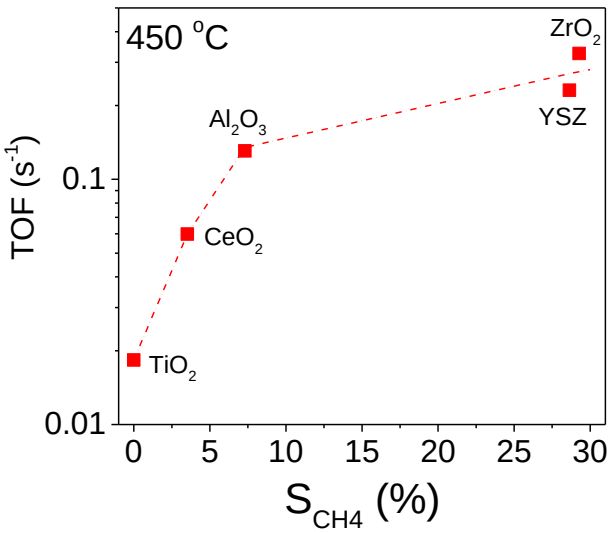

Figure 5. Turnover frequencies of C_3H_8 conversion as a function of selectivity toward CH_4 obtained at 450 °Cover supported Ni catalysts.

It should be mentioned that a different activity order was reported in our previous study over supported Rh catalysts, where it was found that Rh/TiO_2 was the most active catalyst with TOF being one order of magnitude higher compared to that measured for Rh/CeO_2 [11]. This implies that the nature of the metallic phase may affect metal/support interactions leading to variations on propane steam reforming activity and/or possibly changes on the type of active sites on the catalyst surface.

3.3. Long Term Stability Test

The long-term stability of Ni/ZrO_2 catalyst, which exhibited the highest activity, was investigated at 650 °C using the same experimental conditions as those used in catalytic performance tests. In this experiment, the catalyst was reduced in situ at 300 °C under 50%H_2/He flow followed by heating at 650 °C. The flow was then switched to the reaction mixture and determination of the conversion of propane and product selectivity started. The system was shut down overnight, while the catalyst was kept at room temperature under a He flow. The next day the catalyst is heated to 650 °C in the He flow, followed by switching of the flow to the reaction mixture and determination of X_{C3H8} and the product selectivity as a function of time. Results obtained are shown in Figure 6, where X_{C3H8} and S_{H2}, S_{CO2}, S_{CO} and S_{CH4} are plotted as functions of time-on-stream. As it can be seen the catalyst presents excellent stability for more than 30 h-on-stream. Propane conversion and hydrogen selectivity were varied in the range of 95–99% and 97–98%, respectively. The selectivity toward methane was low (3–4%) whereas S_{CO} and S_{CO2} exhibited similar values ranging between 46 and 50%. The carbon balance was found to be satisfactory during the stability test, with a deviation lower than 1–2%.

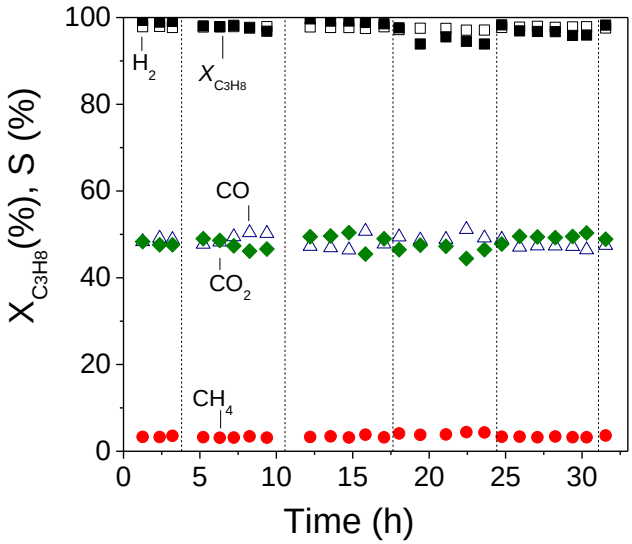

Figure 6. Long-term stability test of the 5%Ni/ZrO_2 catalyst at 650 °C: Alterations of the conversion of C_3H_8 and selectivities toward reaction products with time-on-stream. Experimental conditions: Same as in Figure 3. Dashed vertical black lines indicate shutting down of the system overnight.

3.4. DRIFT Studies

The interaction of selected catalysts with the reaction mixture was also investigated employing in situ FTIR spectroscopy. Experiments were conducted in the temperature range of 100–500 °C using a feed composition of 0.5%C_3H_8 + 5%H_2O (in He) and the results obtained are shown in Figure 7. It is observed that the spectrum recorded at 100 °C (Figure 7A, trace a) for the pre-reduced Ni/TiO_2 catalyst is characterized by two negative bands at 3787 and 3676 cm^{-1} which can be attributed to losses of ν (OH) intensity of at least two different types of free hydroxyl groups, which are either originally present on TiO_2 surface or created via H_2O adsorption. Two weak peaks were also detected in the ν (C-H) region, located at 2987 and 2966 cm^{-1} (trace a) due to C-H stretching vibrations in methyl groups ($CH_{3,ad}$) and to symmetric C-H vibrations in methylene groups ($CH_{2,ad}$), respectively [20,31,34–36]. These peaks are more obvious in Figure 8A (trace a) where selected spectra in the narrow range of 3200–2400 cm^{-1} are presented. Moreover, a band at 1642 cm^{-1} followed by a shoulder at 1560 cm^{-1} can be discerned, which have been previously assigned to carbonate species associated with TiO_2 support [37–42]. An increase of temperature results in progressive separation of the latter two bands which are both shifted toward lower wavenumbers. A new band at 1430 cm^{-1} can be also discerned in the spectra obtained at 350 °C (trace f) which is also due to carbonate species. This peak may be also present in the spectra obtained at lower temperatures but couldn't be clearly observed due to the low signal-to-noise ratio in the region below 1700 cm^{-1}. The intensities of bands assigned to carbonate species are progressively decreased above 200 °C. This decrease is accompanied by the detection of a weak peak at 2021 cm^{-1} [38,43–46], which is characteristic of linear-bonded CO on reduced nickel sites (Ni°), indicating that carabonate species are further decomposed yielding CO and most possibly also CO_2 in the gas phase. The weak bands in the ν (C-H) region are present on the spectra obtained up to 500 °C (Figure 7A, trace i) implying that CH_x species are thermally stable and remained adsorbed on the catalyst surface.

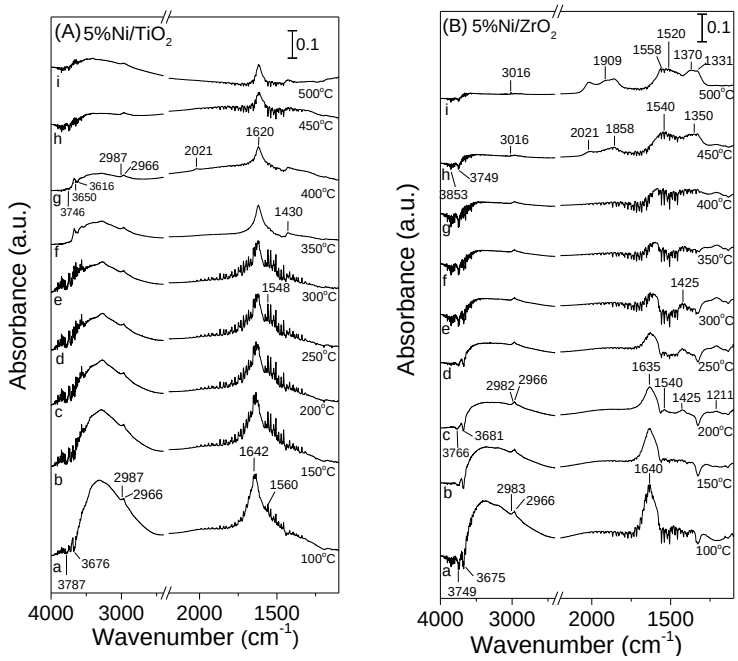

Figure 7. DRIFT spectra obtained over the (**A**) Ni/TiO_2 and (**B**) Ni/ZrO_2 catalysts following interaction with 0.5% C_3H_8 + 5% H_2O (in He) at 100 °C for 15 min and subsequent stepwise heating at 500 °C.

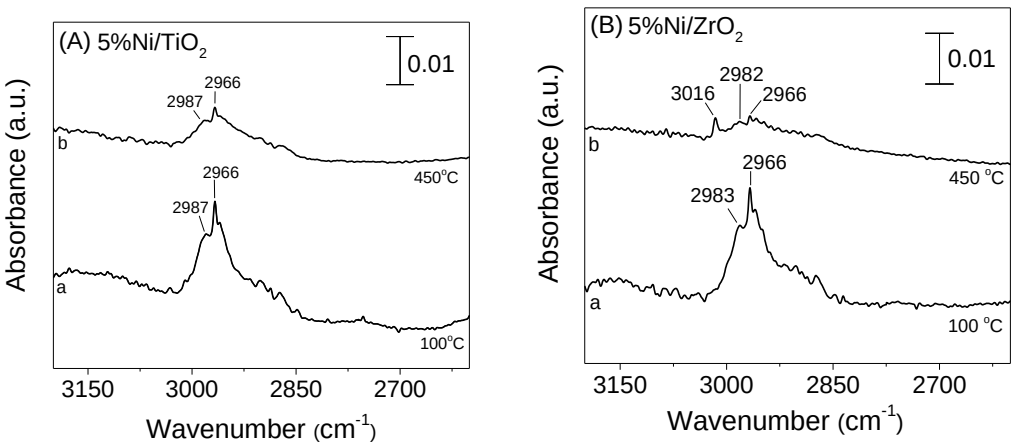

Figure 8. DRIFT spectra obtained in the region 3200–2400 cm^{-1} over the (**A**) Ni/TiO_2 and (**B**) Ni/ZrO_2 catalysts following interaction with 0.5% C_3H_8 + 5% H_2O (in He) at 100 °C and 450 °C for 15 min.

A similar experiment was conducted over the most active Ni/ZrO_2 catalyst and the results obtained are presented in Figure 7B. It is observed that the interaction of catalyst with the reformate mixture at 100 °C (trace a) results in the appearance of bands corresponding to bicarbonate species (1640 cm^{-1}) [47–49], CH_x species (2983 and 2966 cm^{-1}) [31,36,47] as well as by negative bands (3749 and 3675 cm^{-1}) related to the consumption of surface OH groups [31,36,48]. Increase of temperature at 200 °C (trace c) leads to the progressive development of two bands at 1540 and 1425 cm^{-1} due to bicarbonate species [47–49]. The intensity of the latter bands increases with increasing temperature up to 300 °C and diminishes upon further heating at 350–400 °C. This is also the case for the band at 1640 cm^{-1}, indicating that bicarbonate species are decomposed above 450 °C. At temperatures higher than 400 °C (traces h-i) two new broad bands seem to be developed at ca 1540 and 1350 cm^{-1}. The broadness of these bands implies that they may contain contributions from more than one species with their corresponding bands being overlapped.

This can be clearly seen in the spectrum obtained at 500 °C (trace i) where four bands can be clearly discerned located at 1558, 1520, 1370 and 1331 cm^{-1}. Those detected at 1520

and 1331 cm^{-1} have been previously attributed to bidentate carbonates [49,50], whereas those located at 1558 and 1370 cm^{-1} can be assigned to bidentate formate species [51] adsorbed on ZrO_2 surface. The appearance of the latter bands is accompanied by evolution of three peaks in the ν(CO) region due to CO linearly adsorbed on reduced Ni sites (2021 cm^{-1}) and bridged bonded CO (1909 and 1858 cm^{-1}) [43,46,52–54].

Interestingly, CH_x species are eliminated from the spectra obtained above 400 °C followed by evolution of CH_4 in the gas phase, as evidenced by the detection of the 3016 cm^{-1} band (traces h–i). Production of CH_4 at the expense of CH_x species can be clearly seen in Figure 8B where the spectra obtained at 100 and 450 °C in the wavenumber range of 3200–2400 cm^{-1} are presented.

Based on the above it can be suggested that the reaction of steam reforming of propane over Ni/ZrO_2 catalyst proceeds via a dissociative adsorption of propane on metallic Ni leading to the formation of C_3H_x species, which are further decomposed toward CH_x species and probably carbon oxides due to the presence of H_2O adsorbed on the support surface. This may result in the formation of the bicarbonate species (1640, 1540 and 1425 cm^{-1}) detected at low temperatures on the surface of the support [20]. Part of CH_x species are hydrogenated above 400 °C, yielding methane in the gas phase (band at 3016 cm^{-1}) whereas the rest interact with adsorbed water producing formates (bands at 1558 and 1370 cm^{-1}) and, eventually, CO species adsorbed on the Ni surface (bands at 2021, 1909 and 1858 cm^{-1}). Formates may also interact with hydroxyl groups producing H_2 and carbonate species (1520 and 1331 cm^{-1}), which are further decomposed to CO_2 [20]. It should be noted, however, that, under certain conditions, CH_x species may be also dehydrogenated producing C and H_2. Surface carbon is either accumulated on the catalyst surface resulting in catalyst deactivation (which is not the case here) or it interacts with the hydroxyl groups or the lattice oxygen of the support yielding CO or CO_2 [3,16,19,31,55].

The ability of CH_x species to be converted to methane and/or formates on the surface of Ni/ZrO_2 may imply that CH_x species are more weakly adsorbed and/or more reactive on the surface of this catalyst, thus resulting in higher overall activity for the propane steam reforming reaction. This agrees well with results of Figure 5, where it was shown that catalytic activity increases progressively with increasing methane selectivity. If as discussed above the origin of adsorbed CO is formate species, the high reactivity of CH_x species over Ni/ZrO_2 is also indirectly confirmed by the significantly higher population of carbonyl species observed over this catalyst. On the other hand, although CH_x species were also detected on the surface of Ni/TiO_2 catalyst, no band due to gas phase methane or formate species was observed, indicating that CH_x species cannot be further converted in the temperature range investigated. The increase of S_{CH4} in parallel with the increase of catalytic activity (Figure 5) indicates that the reactivity of CH_x species is strongly related to the conversion of propane to the desired products. Although detailed mechanistic studies should be conducted to further explore the reaction pathway, it can be suggested that CH_x species are key reaction intermediates for the reaction of propane steam reforming.

4. Conclusions

The results of the present study show that the catalytic activity of Ni and the product distribution for the propane steam reforming reaction depend strongly on the nature of the support. The specific reaction rate measured for Ni/ZrO_2 catalyst was found to be more than one order of magnitude higher compared to that measured for Ni/TiO_2. The intermediate production of CH_4 is strongly influenced by the type of metal oxide used as support following the same trend with that of catalytic activity. DRIFTS studies provided evidences that the most active Ni/ZrO_2 catalyst is able to convert the intermediate produced CH_x species to CH_4 and/or formate species and, subsequently, to carbon oxides and H_2. In contrast, CH_x species seem to be less reactive when Ni is dispersed on TiO_2, thus resulting in a lower reaction rate. In addition to the high activity of Ni/ZrO_2 catalyst, it was also found to be stable for more than 30 h on stream and therefore, is a promising candidate for the production of H_2 for fuel cell applications.

Author Contributions: Conceptualization, P.P.; methodology, P.P.; investigation, A.K., A.P. and P.P.; data curation, A.K., A.P. and P.P.; writing—original draft preparation, P.P.; writing—review and editing, P.P.; visualization, P.P.; supervision, P.P.; project administration, P.P.; funding acquisition, P.P. All authors have read and agreed to the published version of the manuscript.

Funding: This research has been co-financed by the European Union and Greek national funds through the Operational Program Competitiveness, Entrepreneurship and Innovation, under the call RESEARCH–CREATE–INNOVATE (project code: T1EDK–02442).

Institutional Review Board Statement: Not applicable.

Informed Consent Statement: Not applicable.

Data Availability Statement: Not applicable.

Conflicts of Interest: The authors declare no conflict of interest. The funders had no role in the design of the study; in the collection, analyses, or interpretation of data; in the writing of the manuscript, or in the decision to publish the results.

References

1. Kalamaras, C.M.; Efstathiou, A.M. Hydrogen Production Technologies: Current State and Future Developments. *Conf. Pap. Energy* **2013**, *2013*, 690627. [CrossRef]
2. Nikolaidis, P.; Poullikkas, A. A comparative overview of hydrogen production processes. *Renew. Sustain. Energy Rev.* **2017**, *67*, 597–611. [CrossRef]
3. Im, Y.; Lee, J.H.; Kwak, B.S.; Do, J.Y.; Kang, M. Effective hydrogen production from propane steam reforming using M/NiO/YSZ catalysts (M = Ru, Rh, Pd, and Ag). *Catal. Today* **2018**, *303*, 168–176. [CrossRef]
4. Santamaria, L.; Lopez, G.; Arregi, A.; Amutio, M.; Artetxe, M.; Bilbao, J.; Olazar, M. Influence of the support on Ni catalysts performance in the in-line steam reforming of biomass fast pyrolysis derived volatiles. *Appl. Catal. B Environ.* **2018**, *229*, 105–113. [CrossRef]
5. Santamaria, L.; Lopez, G.; Arregi, A.; Amutio, M.; Artetxe, M.; Bilbao, J.; Olazar, M. Stability of different Ni supported catalysts in the in-line steam reforming of biomass fast pyrolysis volatiles. *Appl. Catal. B Environ.* **2019**, *242*, 109–120. [CrossRef]
6. Miyazawa, T.; Kimura, T.; Nishikawa, J.; Kado, S.; Kunimori, K.; Tomishige, K. Catalytic performance of supported Ni catalysts in partial oxidation and steam reforming of tar derived from the pyrolysis of wood biomass. *Catal. Today* **2006**, *115*, 254–262. [CrossRef]
7. Al-Zuhair, S.; Hassan, M.; Djama, M.; Khaleel, A. Hydrogen Production by Steam Reforming of Commercially Available LPG in UAE. *Chem. Eng. Commun.* **2017**, *204*, 141–148. [CrossRef]
8. Do, J.Y.; Lee, J.H.; Park, N.-K.; Lee, T.J.; Lee, S.T.; Kang, M. Synthesis and characterization of Ni2−xPdxMnO4/γ-Al_2O_3 catalysts for hydrogen production via propane steam reforming. *Chem. Eng. J.* **2018**, *334*, 1668–1678. [CrossRef]
9. Do, J.Y.; Park, N.-K.; Lee, T.J.; Lee, S.T.; Kang, M. Effective hydrogen productions from propane steam reforming over spinel-structured metal-manganese oxide redox couple catalysts. *Int. J. Energy Res.* **2018**, *42*, 429–446. [CrossRef]
10. Barzegari, F.; Kazemeini, M.; Farhadi, F.; Rezaei, M.; Keshavarz, A. Preparation of mesoporous nanostructure NiO–MgO–SiO2 catalysts for syngas production via propane steam reforming. *Int. J. Hydrogen Energy* **2020**, *45*, 6604–6620. [CrossRef]
11. Kokka, A.; Katsoni, A.; Yentekakis, I.V.; Panagiotopoulou, P. Hydrogen production via steam reforming of propane over supported metal catalysts. *Int. J. Hydrogen Energy* **2020**. [CrossRef]
12. Kokka, A.; Ramantani, T.; Panagiotopoulou, P. Effect of Operating Conditions on the Performance of Rh/TiO_2 Catalyst for the Reaction of LPG Steam Reforming. *Catalysts* **2021**, *11*, 374. [CrossRef]
13. Yu, L.; Sato, K.; Nagaoka, K. Rh/Ce0.25Zr0.75O2 Catalyst for Steam Reforming of Propane at Low Temperature. *ChemCatChem* **2019**, *11*, 1472–1479. [CrossRef]
14. Karakaya, C.; Karadeniz, H.; Maier, L.; Deutschmann, O. Surface Reaction Kinetics of the Oxidation and Reforming of Propane over Rh/Al_2O_3 Catalysts. *ChemCatChem* **2017**, *9*, 685–695. [CrossRef]
15. Aghamiri, A.R.; Alavi, S.M.; Bazyari, A.; Azizzadeh Fard, A. Effects of simultaneous calcination and reduction on performance of promoted Ni/SiO2 catalyst in steam reforming of propane. *Int. J. Hydrogen Energy* **2019**, *44*, 9307–9315. [CrossRef]
16. Harshini, D.; Yoon, C.W.; Han, J.; Yoon, S.P.; Nam, S.W.; Lim, T.-H. Catalytic Steam Reforming of Propane over Ni/LaAlO3 Catalysts: Influence of Preparation Methods and OSC on Activity and Stability. *Catal. Lett.* **2012**, *142*, 205–212. [CrossRef]
17. Azizzadeh Fard, A.; Arvaneh, R.; Alavi, S.M.; Bazyari, A.; Valaei, A. Propane steam reforming over promoted Ni–Ce/MgAl2O4 catalysts: Effects of Ce promoter on the catalyst performance using developed CCD model. *Int. J. Hydrogen Energy* **2019**, *44*, 21607–21622. [CrossRef]
18. Kim, K.M.; Kwak, B.S.; Park, N.-K.; Lee, T.J.; Lee, S.T.; Kang, M. Effective hydrogen production from propane steam reforming over bimetallic co-doped NiFe/Al_2O_3 catalyst. *J. Ind. Eng. Chem.* **2017**, *46*, 324–336. [CrossRef]

19. Laosiripojana, N.; Sangtongkitcharoen, W.; Assabumrungrat, S. Catalytic steam reforming of ethane and propane over CeO_2-doped Ni/Al_2O_3 at SOFC temperature: Improvement of resistance toward carbon formation by the redox property of doping CeO_2. *Fuel* **2006**, *85*, 323–332. [CrossRef]
20. Natesakhawat, S.; Oktar, O.; Ozkan, U.S. Effect of lanthanide promotion on catalytic performance of sol–gel Ni/Al_2O_3 catalysts in steam reforming of propane. *J. Mol. Catal. A Chem.* **2005**, *241*, 133–146. [CrossRef]
21. Matsumura, Y.; Nakamori, T. Steam reforming of methane over nickel catalysts at low reaction temperature. *Appl. Catal. A Gen.* **2004**, *258*, 107–114. [CrossRef]
22. Guo, J.; Lou, H.; Zhao, H.; Chai, D.; Zheng, X. Dry reforming of methane over nickel catalysts supported on magnesium aluminate spinels. *Appl. Catal. A Gen.* **2004**, *273*, 75–82. [CrossRef]
23. Lee, D.S.; Min, D.J. A Kinetics of Hydrogen Reduction of Nickel Oxide at Moderate Temperature. *Met. Mater. Int.* **2019**, *25*, 982–990. [CrossRef]
24. Richardson, J.T.; Scates, R.; Twigg, M.V. X-ray diffraction study of nickel oxide reduction by hydrogen. *Appl. Catal. A Gen.* **2003**, *246*, 137–150. [CrossRef]
25. Richardson, J.T.; Scates, R.M.; Twigg, M.V. X-ray diffraction study of the hydrogen reduction of NiO/α-Al_2O_3 steam reforming catalysts. *Appl. Catal. A Gen.* **2004**, *267*, 35–46. [CrossRef]
26. Almasan, V.; Gaeumann, T.; Lazar, M.; Marginean, P.; Aldea, N. Hydrogen spillover effect over the oxide surfaces in supported nickel catalysts. In *Studies in Surface Science and Catalysis*; Froment, G.F., Waugh, K.C., Eds.; Elsevier: Amsterdam, The Netherlands, 1997; Volume 109, pp. 547–552.
27. Kramer, R.; Andre, M. Adsorption of atomic hydrogen on alumina by hydrogen spillover. *J. Catal.* **1979**, *58*, 287–295. [CrossRef]
28. Hatzisymeon, M.; Petala, A.; Panagiotopoulou, P. Carbon Dioxide Hydrogenation over Supported Ni and Ru Catalysts. *Catal. Lett.* **2021**, *151*, 888–900. [CrossRef]
29. Kolb, G.; Zapf, R.; Hessel, V.; Löwe, H. Propane steam reforming in micro-channels—results from catalyst screening and optimisation. *Appl. Catal. A Gen.* **2004**, *277*, 155–166. [CrossRef]
30. Modafferi, V.; Panzera, G.; Baglio, V.; Frusteri, F.; Antonucci, P.L. Propane reforming on Ni–Ru/GDC catalyst: H2 production for IT-SOFCs under SR and ATR conditions. *Appl. Catal. A Gen.* **2008**, *334*, 1–9. [CrossRef]
31. Malaibari, Z.O.; Croiset, E.; Amin, A.; Epling, W. Effect of interactions between Ni and Mo on catalytic properties of a bimetallic Ni-Mo/Al_2O_3 propane reforming catalyst. *Appl. Catal. A Gen.* **2015**, *490*, 80–92. [CrossRef]
32. Helali, Z.; Jedidi, A.; Syzgantseva, O.A.; Calatayud, M.; Minot, C. Scaling reducibility of metal oxides. *Theor. Chem. Acc.* **2017**, *136*, 100–115. [CrossRef]
33. Alphonse, P.; Ansart, F. Catalytic coatings on steel for low-temperature propane prereforming to solid oxide fuel cell (SOFC) application. *J. Colloid Interface Sci.* **2009**, *336*, 658–666. [CrossRef]
34. Panagiotopoulou, P.; Kondarides, D.I.; Verykios, X.E. Mechanistic aspects of the selective methanation of CO over Ru/TiO_2 catalyst. *Catal. Today* **2012**, *181*, 138–147. [CrossRef]
35. Panagiotopoulou, P. Methanation of CO_2 over alkali-promoted Ru/TiO_2 catalysts: II. Effect of alkali additives on the reaction pathway. *Appl. Catal. B Environ.* **2018**, *236*, 162–170. [CrossRef]
36. Wang, B.; Wu, X.; Ran, R.; Si, Z.; Weng, D. IR characterization of propane oxidation on Pt/CeO_2–ZrO_2: The reaction mechanism and the role of Pt. *J. Mol. Catal. A Chem.* **2012**, *356*, 100–105. [CrossRef]
37. Panagiotopoulou, P.; Christodoulakis, A.; Kondarides, D.I.; Boghosian, S. Particle size effects on the reducibility of titanium dioxide and its relation to the water–gas shift activity of Pt/TiO_2 catalysts. *J. Catal.* **2006**, *240*, 114–125. [CrossRef]
38. Kokka, A.; Ramantani, T.; Petala, A.; Panagiotopoulou, P. Effect of the nature of the support, operating and pretreatment conditions on the catalytic performance of supported Ni catalysts for the selective methanation of CO. *Catal. Today* **2020**, *355*, 832–843. [CrossRef]
39. Karelovic, A.; Ruiz, P. Mechanistic study of low temperature CO_2 methanation over Rh/TiO_2 catalysts. *J. Catal.* **2013**, *301*, 141–153. [CrossRef]
40. Liao, L.F.; Lien, C.F.; Shieh, D.L.; Chen, M.T.; Lin, J.L. FTIR Study of Adsorption and Photoassisted Oxygen Isotopic Exchange of Carbon Monoxide, Carbon Dioxide, Carbonate, and Formate on TiO_2. *J. Phys. Chem. B* **2002**, *106*, 11240–11245. [CrossRef]
41. Marwood, M.; Doepper, R.; Renken, A. In-situ surface and gas phase analysis for kinetic studies under transient conditions The catalytic hydrogenation of CO2. *Appl. Catal. A Gen.* **1997**, *151*, 223–246. [CrossRef]
42. Mino, L.; Spoto, G.; Ferrari, A.M. CO2 Capture by TiO_2 Anatase Surfaces: A Combined DFT and FTIR Study. *J. Phys. Chem. C* **2014**, *118*, 25016–25026. [CrossRef]
43. Aldana, P.A.U.; Ocampo, F.; Kobl, K.; Louis, B.; Thibault-Starzyk, F.; Daturi, M.; Bazin, P.; Thomas, S.; Roger, A.C. Catalytic CO_2 valorization into CH_4 on Ni-based ceria-zirconia. Reaction mechanism by operando IR spectroscopy. *Catal. Today* **2013**, *215*, 201–207. [CrossRef]
44. Westermann, A.; Azambre, B.; Bacariza, M.C.; Graça, I.; Ribeiro, M.F.; Lopes, J.M.; Henriques, C. Insight into CO_2 methanation mechanism over NiUSY zeolites: An operando IR study. *Appl. Catal. B Environ.* **2015**, *174–175*, 120–125. [CrossRef]
45. Mohamed, Z.; Dasireddy, V.D.B.C.; Singh, S.; Friedrich, H.B. The preferential oxidation of CO in hydrogen rich streams over platinum doped nickel oxide catalysts. *Appl. Catal. B Environ.* **2016**, *180*, 687–697. [CrossRef]
46. Konishcheva, M.V.; Potemkin, D.I.; Badmaev, S.D.; Snytnikov, P.V.; Paukshtis, E.A.; Sobyanin, V.A.; Parmon, V.N. On the Mechanism of CO and CO_2 Methanation Over Ni/CeO_2 Catalysts. *Top. Catal.* **2016**, *59*, 1424–1430. [CrossRef]

47. Köck, E.-M.; Kogler, M.; Bielz, T.; Klötzer, B.; Penner, S. In Situ FT-IR Spectroscopic Study of CO_2 and CO Adsorption on Y_2O_3, ZrO_2, and Yttria-Stabilized ZrO_2. *J. Phys. Chem. C* **2013**, *117*, 17666–17673. [CrossRef]
48. Bachiller-Baeza, B.; Rodriguez-Ramos, I.; Guerrero-Ruiz, A. Interaction of Carbon Dioxide with the Surface of Zirconia Polymorphs. *Langmuir* **1998**, *14*, 3556–3564. [CrossRef]
49. Zhang, Z.; Zhang, L.; Hülsey, M.J.; Yan, N. Zirconia phase effect in Pd/ZrO_2 catalyzed CO_2 hydrogenation into formate. *Mol. Catal.* **2019**, *475*, 110461. [CrossRef]
50. Föttinger, K.; Emhofer, W.; Lennon, D.; Rupprechter, G. Adsorption and Reaction of CO on (Pd–)Al_2O_3 and (Pd–)ZrO_2: Vibrational Spectroscopy of Carbonate Formation. *Topics Catal.* **2017**, *60*, 1722–1734. [CrossRef] [PubMed]
51. Pokrovski, K.; Jung, K.T.; Bell, A.T. Investigation of CO and CO_2 Adsorption on Tetragonal and Monoclinic Zirconia. *Langmuir* **2001**, *17*, 4297–4303. [CrossRef]
52. Anderson, J.A.; Daza, L.; Fierro, J.L.G.; Rodrigo, M.T. Influence of preparation method on the characteristics of nickel/sepiolite catalysts. *J. Chem. Soc. Faraday Trans.* **1993**, *89*, 3651–3657. [CrossRef]
53. Wu, R.-f.; Zhang, Y.; Wang, Y.-z.; Gao, C.-g.; Zhao, Y.-x. Effect of ZrO_2 promoter on the catalytic activity for CO methanation and adsorption performance of the Ni/SiO_2 catalyst. *J. Fuel Chem. Technol.* **2009**, *37*, 578–582. [CrossRef]
54. Zhou, G.; Liu, H.; Cui, K.; Jia, A.; Hu, G.; Jiao, Z.; Liu, Y.; Zhang, X. Role of surface Ni and Ce species of Ni/CeO_2 catalyst in CO_2 methanation. *Appl. Surf. Sci.* **2016**, *383*, 248–252. [CrossRef]
55. Faria, E.C.; Rabelo-Neto, R.C.; Colman, R.C.; Ferreira, R.A.R.; Hori, C.E.; Noronha, F.B. Steam Reforming of LPG over Ni/Al_2O_3 and Ni/CexZr1—xO2/Al_2O_3 Catalysts. *Catal. Lett.* **2016**, *146*, 2229–2241. [CrossRef]